Am J Physiol Heart Circ Physiol 295: H245–H255, 2008.
First published May 16, 2008; doi:10.1152/ajpheart.00066.2008.

Diacylglycerol kinase-ε restores cardiac dysfunction under chronic pressure overload: a new specific regulator of $G\alpha_q$ signaling cascade

Takeshi Niizeki,[1] Yasuchika Takeishi,[4] Tatsuro Kitahara,[1] Takanori Arimoto,[1] Mitsunori Ishino,[1] Olga Bilim,[1] Satoshi Suzuki,[1] Toshiki Sasaki,[1] Osamu Nakajima,[2] Richard A. Walsh,[5] Kaoru Goto,[3] and Isao Kubota[1]

[1]*Department of Cardiology, Pulmonology, and Nephrology,* [2]*Research Laboratory for Molecular Genetics, and* [3]*Department of Anatomy and Cell Biology, Yamagata University School of Medicine, Yamagata, and* [4]*First Department of Internal Medicine, Fukushima Medical University, Fukushima, Japan; and* [5]*Department of Medicine, Case Western Reserve University, Cleveland, Ohio*

Submitted 22 January 2008; accepted in final form 13 May 2008

Niizeki T, Takeishi Y, Kitahara T, Arimoto T, Ishino M, Bilim O, Suzuki S, Sasaki T, Nakajima O, Walsh RA, Goto K, Kubota I. Diacylglycerol kinase-ε restores cardiac dysfunction under chronic pressure overload: a new specific regulator of $G\alpha_q$ signaling cascade. *Am J Physiol Heart Circ Physiol* 295: H245–H255, 2008. First published May 16, 2008; doi:10.1152/ajpheart.00066.2008.—$G\alpha_q$ protein-coupled receptor (GPCR) signaling pathway, which includes diacylglycerol (DAG) and protein kinase C (PKC), plays a critical role in cardiac hypertrophy. DAG kinase (DGK) catalyzes DAG phosphorylation and controls cellular DAG levels, thus acting as a regulator of GPCR signaling. It has been reported that DGKε acts specifically on DAG produced by inositol cycling. In this study, we examined whether DGKε prevents cardiac hypertrophy and progression to heart failure under chronic pressure overload. We generated transgenic mice with cardiac-specific overexpression of DGKε (DGKε-TG) using an α-myosin heavy chain promoter. There were no differences in cardiac morphology and function between wild-type (WT) and DGKε-TG mice at the basal condition. Either continuous phenylephrine infusion or thoracic transverse aortic constriction (TAC) was performed in WT and DGKε-TG mice. Increases in heart weight after phenylephrine infusion and TAC were abolished in DGKε-TG mice compared with WT mice. Cardiac dysfunction after TAC was prevented in DGKε-TG mice, and the survival rate after TAC was higher in DGKε-TG mice than in WT mice. Phenylephrine- and TAC-induced DAG accumulation, the translocation of PKC isoforms, and the induction of fetal genes were blocked in DGKε-TG mouse hearts. The upregulation of transient receptor potential channel (TRPC)-6 expression after TAC was attenuated in DGKε-TG mice. In conclusion, these results demonstrate the first evidence that DGKε restores cardiac dysfunction and improves survival under chronic pressure overload by controlling cellular DAG levels and TRPC-6 expression. DGKε may be a novel therapeutic target to prevent cardiac hypertrophy and progression to heart failure.

hypertrophy; heart failure; diacylglycerol; protein kinase C

CARDIOVASCULAR DISEASE REPRESENTS an important and growing public health problem and is the cause of substantial morbidity and mortality. Cardiac hypertrophy is initially a compensatory response to a variety of stimuli such as chronic hypertension, stenotic valves, and loss of contractile mass from previous myocardial infarction. Conversely, sustained cardiac hypertrophy can eventually lead to decompensation characterized by heart failure, arrhythmias, and cardiac death (16). Therefore, the identification of novel molecular mechanisms underlying the development of cardiac hypertrophy and its transition to heart failure is an important challenge of cardiovascular biology and medicine. Multiple lines of experimental and clinical evidence have suggested the importance of the $G\alpha_q$ protein-coupled receptor (GPCR) signaling in the development of pathological cardiac hypertrophy and heart failure (11, 31). GPCR agonists such as angiotensin II (25), endothelin-1 (26), and phenylephrine (20) activate phospholipase C (PLC)-mediated hydrolysis of phosphatidylinositol 4,5-bisphosphate, which produces inositol 1,4, 5-trisphosphate and diacylglycerol (DAG). DAG functions as a potent activator of protein kinase C (PKC). We and others have previously demonstrated that PKC plays an important role in the development of cardiac hypertrophy and progression to heart failure (3, 30, 32).

One major route for terminating DAG signaling is thought to be its phosphorylation and inactivation by DAG kinase (DGK), producing phosphatidic acid (PA) (7, 14, 33). Three DGK isoforms, α, ε, and ζ, are expressed in the heart, and we have recently demonstrated in cultured rat neonatal cardiomyocytes that adenoviral-mediated expression of DGKζ blocks endothelin-1-induced increases in cell size and the reactivation of fetal genes via the inhibition of PKCε extracellular signal-regulated kinase (ERK)-activator protein-1 (AP-1) signaling pathway (28). Furthermore, we have generated transgenic mice with cardiac-specific overexpression of DGKζ using an α-myosin heavy chain (MHC) promoter and demonstrated that DGKζ negatively regulates the hypertrophic signaling cascade and resultant cardiac hypertrophy after GPCR agonist infusion without any detectable adverse effects in in vivo hearts (1). On the other hand, it has been reported that DGKε acts specifically on DAG produced by inositol cycling compared with DGKζ, suggesting differences in two DGK isoforms about substrate specificity and the functional roles in signal transduction pathway (22). In addition, there are differences in subcellular localization between two isoforms, DGKζ in the nucleus and DGKε in cytoplasm (14). In this study, to characterize the functional role of DGKε in the heart, we generated transgenic mice with cardiac-specific overexpression of DGKε (DGKε-TG) using an α-MHC promoter and examined whether DGKε prevents cardiac hypertrophy and progression to heart failure under chronic pressure overload. We demonstrated that DGKε

Address for reprint requests and other correspondence: T. Niizeki, Dept. of Cardiology, Pulmonology, and Nephrology, Yamagata Univ. School of Medicine, 2-2-2 Iida-Nishi, Yamagata, Japan 990-9585 (e-mail: tniizeki@nihonkai.gr.jp).

The costs of publication of this article were defrayed in part by the payment of page charges. The article must therefore be hereby marked "*advertisement*" in accordance with 18 U.S.C. Section 1734 solely to indicate this fact.

restores cardiac dysfunction and improves survival under chronic pressure overload by controlling cellular DAG levels and transient receptor potential channel (TRPC)-6 expression.

METHODS

Generation of DGKε-TG mice. DGKε-TG mice were created in Yamagata University by standard techniques as described previously (1). Briefly, a 5.5-kb fragment of murine α-MHC gene promoter (a kind gift from Dr J. Robbins, Children's Hospital Research Foundation, Cincinnati, OH) and rat DGKε cDNA (7) were subcloned into pBSIISK (+) plasmids. The plasmid was digested with *Spe*I to generate a DNA fragment composed of the α-MHC gene promoter, DGKε cDNA, and a poly-A tail of the human growth hormone, as illustrated in Fig. 1*A*. We microinjected the DNA construct into the pronuclei of single-cell fertilized mouse embryos to generate transgenic mice as previously described (1). To detect the exogenous DGKε gene, genomic DNA was extracted from the tail tissues of 4-wk-old pups, and polymerase chain reaction (PCR) was performed with one primer specific for the α-MHC gene promoter and another primer specific for the DGKε, as shown in Fig. 1*A*.

Wild-type (WT) littermate mice and DGKε-TG mice aged 8–10-wk old with a BDF1 background were used in the present study. Mice were housed in a facility with a 12-h:12-h light-dark cycle and were given free access to water and standard rodent chow. The room was kept specific pathogen-free. All experimental procedures were performed according to the animal welfare regulations of Yamagata University School of Medicine, and the study protocol was approved by the Animal Subjects Committee of Yamagata University School of Medicine. The investigation conformed to the *Guide for the Care and Use of Laboratory Animals* published by the National Institutes of Health.

Western blot analysis. Membranous and cytosolic fractions of detergent-extracted PKC were prepared from the left ventricular myocardium as described previously (1, 30, 31). The protein concentration of myocardial samples was carefully determined by the protein assay, and equal amounts of protein were subjected to 10% SDS-PAGE electrophoresis and transferred to polyvinylidene difluoride membranes. To ensure an equivalent protein loading and quantitative transfer efficiency of proteins, the membranes were stained with Ponceau S before incubating with primary antibodies. The subcellular localization of PKC isoforms was examined by quantitative immunoblotting using isoform-specific antibodies (mouse monoclonal anti-PKCα, β, δ, and ε, Santa Cruz Biotechnology, Santa Cruz, CA) as reported previously (1, 30, 31). Immunoreactive bands were detected by an enhanced chemiluminescence (ECL) kit (Amersham Biosciences, Piscataway, NJ), and membrane-to-cytosol ratios of immunoreactivity were used as indexes for the extent of translocation of PKC isoforms.

We prepared total protein from the left ventricular myocardium using a cell lysis buffer (Cell Signaling Technology, Danvers, MA) to examine protein expressions of TRPC isoforms. TRPC isoforms (TRPC 1, 3, 4, and 6) expressions were examined by quantitative immunoblotting using isoform-specific antibodies (Sigma, St. Louis, MO). Immunoreactive bands were detected by an ECL kit, and TRPC isoform expressions were normalized to actin.

We prepared nuclear and cytosolic protein from left ventricular myocardium using a nuclear and cytoplasmic extraction reagents (Pierce, Tokyo, Japan) to examine localization of DGK isoforms.

Real-time RT-PCR. Total RNAs were extracted from the left ventricle using TRIzol (Invitrogen, Tokyo, Japan), and first-strand cDNA was synthesized from 1 μg of RNA sample with oligo (dT) primers and superscript II RT as previously described (1, 28). To examine mRNA expression levels of DGKε, atrial natriuretic factor (ANF), β-MHC, brain natriuretic peptide (BNP), α-skeletal actin, collagen type I, collagen type III, and TRPC isoforms (TRPC 1, 3, 4, and 6), real-time RT-PCR amplification was performed as reported previously (1, 28). Standard curves of these genes were generated by full-sequence plasmid of known concentrations. Gene expressions were normalized to glyceraldehyde-3-phosphate dehydrogenase (GAPDH). Primers were designed based on GenBank sequences (ANF, K-02781; β-MHC, AY-056464; BNP, NM-008726; α-skeletal actin, NM-009606; collagen type I, NM-007742; collagen type III, NM-009930; TRPC 1, NM-011643; TRPC 3, NM-019510; TRPC 4, NM-016984; TRPC 6, NM-013838; and GAPDH, NM-001001303). Sense and anti-sense primers for DGKε were 5'-TTCCTTCCTAG-CATTGTGTG-3' and 5'-AGGTCCAGGAAGATGAAACA-3'. The reaction conditions for the RT are a denaturing step at 95°C for 10 min followed by a three-step PCR amplification to quantify expression. The steps are 95°C for 10 s, 55–62°C for 10 s, and 72°C for 5–9 s (depending on the gene) for 45 cycles.

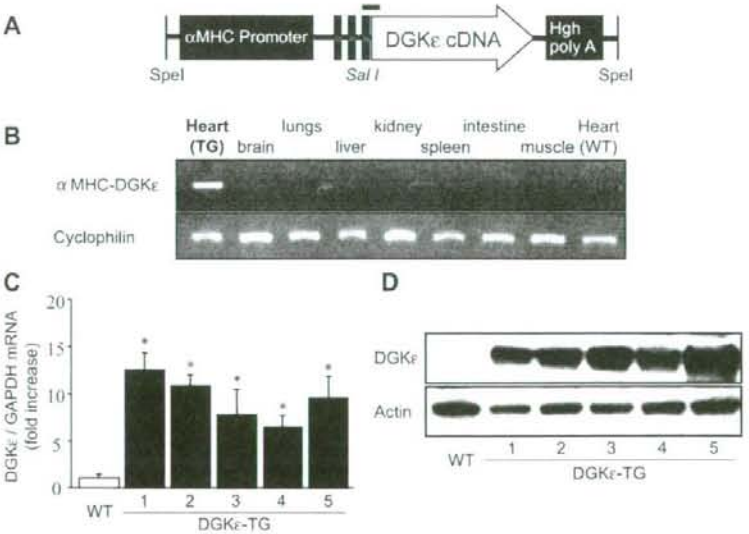

Fig. 1. *A*: transgene construct used for the generation of diacylglycerol (DAG) kinase-transgenic (DGKε-TG) mice. The transgene contains the α-myosin heavy chain (MHC) gene promoter, the full-length rat DGKε cDNA clone, and a human growth hormone (Hgh) poly-A sequence. Solid line, region amplified by PCR for genotyping. *B*: cardiac-specific expression of transgene was confirmed by RT-PCR. *C*: quantitative analysis of DGKε mRNA expression of wild-type (WT) and DGKε-TG mice by real-time RT-PCR. Data are reported as means ± SE obtained from 6 mice for each group. * $P < 0.05$ vs. WT mice. *D*: representative Western blots of DGKε protein from WT and DGKε-TG mouse hearts.

Lipid extraction and measurements of myocardial DAG levels. Myocardial lipid extract was prepared from the left ventricle, and DAG levels were measured as previously reported (1). Briefly, with the use of the DAG within myocardial lipid extract as substrate and with the use of [γ-^{32}P]ATP, the myocardial DAG level was quantified by production of [^{32}P]PA. After 30 min of incubation, the reaction was terminated and the radiolabeled product was separated by thin-layer chromatography on silica plates. The [^{32}P]PA was identified by autoradiography. Silica corresponding to PA was scraped and counted by liquid scintillation counting (1).

Caspase-3 activity. Caspase-3 activity in myocardial tissues was measured with a APOPCYTO/caspase-3 colorimetric assay kit (Medical & Biological Laboratories, Nagoya, Japan) that recognizes the sequence DEVD. The assay was from the labeled substrate DEVD-p-nitroanilide.

Subcutaneous implantation of osmotic minipump and thoracic transverse aortic constriction. A subpressor dose of phenylephrine (20 mg·kg^{-1}·day^{-1}) dissolved in saline or saline alone (control) was continuously infused into mice subcutaneously via an osmotic minipump (ALZET Osmotic Pump, DURECT) for 3 days. This dose did not increase systolic blood pressure as previous studies (1, 20). Systolic blood pressure was determined in the conscious state with the use of a computerized tail-cuff monometer, MK-1030 (Muromachi Kikai), as reported previously (1).

Thoracic transverse aortic constriction (TAC) was performed to produce chronic pressure overload as described previously (9). Briefly, mice (20–25 g body wt) were anesthetized and intubated with a 20-gauge polyethylene catheter and ventilated with a rodent ventilator (Harvard Apparatus, Holliston, MA). The chest cavity was opened at the second intercostals space at the left upper sternal border. The transverse section of the aorta was freed, an 8-0 prolene suture was passed around the aorta between the right innominate and left common carotid arteries, a tight ligature was tied against a 27-gauge needle, and the needle was then promptly removed. In sham-operated animals, the same procedure was performed except for the ligation. Finally, the lungs were reexpanded, and the chest wall was closed. The animals remained in a supervised setting until fully conscious.

Echocardiography and cardiac catheterization. Transthoracic echocardiography was recorded as described previously with an FFsonic 8900 (Fukuda Denshi, Tokyo, Japan) equipped with a 13-MHz phased-array transducer (1, 9). Left ventricular internal dimensions at end systole and end diastole (LVESD and LVEDD, respectively), interventricular septum (IVS), and left ventricular posterior wall thickness (PW) were measured digitally on the M-mode tracings and averaged from at least three cardiac cycles. Left ventricular fractional shortening (LVFS) was calculated as [(LVEDD − LVESD)/LVEDD] × 100.

A closed-chest approach by cardiac catheter was performed as described previously (40). The right carotid artery was cannulated under anesthesia by the micropressure transducer with an outer diameter of 0.42 mm (Samba 3200, Samba Sensors, Göteborg, Sweden), which was then advanced into the left ventricle. Heart rate, left ventricular end-diastolic pressure (LVEDP) and end-systolic pressure, the maximal and minimum rates of left ventricular pressure development ($\pm$dP/dt), and the time constant of left ventricular isovolumic relaxation (τ) were measured using an Acknowledge version 3.8.1 system with a sampling rate of 2,000 Hz (37).

Morphological and histopathological examinations. After mice were euthanized, the coronary arteries were retrogradely flushed with saline and the heart, lungs, and liver were excised and weighed. The heart was fixed with a 10% solution of formalin in PBS at 4°C for 24 h, embedded in paraffin, and then cut serially from the apex to the base. The sections were stained with hematoxylin-eosin or Masson's trichrome stain for histopathological analysis. Transverse sections were captured digitally, and cardiomyocyte cross-sectional area was measured using a Scion imaging system (Scion, Frederick, MD) (9). We traced the outline of at least 200 cardiomyocytes in each section, and the data were averaged.

To assess the degree of fibrosis, the sections stained with Masson's trichrome stain were scanned with computer-assisted videodensitometry, and the images from at least 10 fields for each heart were analyzed. The fibrosis fraction was obtained by calculating the ratio of Masson's trichrome-stained connective tissue area (stained blue) to total myocardial area (stained red) with image analysis software as described previously (9).

In immunohistochemical analysis, myocardial sections from DGKε-TG and DGKζ-TG (1) mice were stained with anti-DGKε and anti-DGKζ antibodies, respectively, to examine the differences in subcellular localization of two DGK isoforms. The staining was visualized by treatment for 15–20 s in the solution of 3,3′-diaminobenzidine (Dako Cytomation Liquid DAB Substrate Chromogen System, Dako Japan, Tokyo, Japan). Control reactions included the omission of the primary antibody, which was substituted by nonimmune rabbit serum.

Statistical analysis. All values are reported as means ± SE. The effects of phenylephrine or TAC on gravimetric data, histological data, PKC translocation, TRPC isoform expressions, echocardiographic data, cardiac catheter data, and RT-PCR data between WT and DGKε-TG mice were analyzed by two-way ANOVA or the Friedman test followed by multiple comparisons with the Fisher protected least significant difference test. Survival curves were created by the Kaplan-Meier method and compared by a log-rank test. A value of $P < 0.05$ was considered statistically significant.

RESULTS

Cardiac-specific overexpression of DGKε does not affect cardiac function at basal condition. After microinjection and embryo implantation, five transgenic mice lines were successfully established. Cardiac-specific expression of transgene was confirmed by RT-PCR as shown in Fig. 1*B*. We confirmed the expression levels of DGKε in the left ventricle by real-time RT-PCR (Fig. 1*C*) and Western blot analysis (Fig. 1*D*) in five DGKε-TG lines. Among them, *line 2* with the moderate expression level and high-breeding capacity was characterized in the following experiments.

Both male and female DGKε-TG mice had normal life spans and no evidence of morphogenic defects in cardiac or skeletal muscle. To characterize mouse phenotypes, all experiments were performed with age- and sex-matched (8–10 wk old) WT littermate mice and DGKε-TG mice. Body weight, systolic blood pressure, and heart rate were similar between WT and DGKε-TG mice. The absolute heart weight, ratio of heart weight to body weight, and ratio of the left ventricular weight to body weight were not different between WT and DGKε-TG mice. Echocardiography demonstrated that cardiac dimensions, wall thickness, and LVFS were normal in DGKε-TG mice. There was no evidence of fibrosis on microscopic examinations of multiple histological sections. In immunohistochemical staining and Western blot analysis, we detected differences in subcellular localization between DGK isoforms in cardiomyocytes from hearts of DGKζ-TG and DGKε-TG mice, DGKζ in the nucleus, and DGKε in cytoplasm and nucleus as shown in Fig. 2.

Effects of DGKε on hypertrophic programs in response to phenylephrine infusion. WT and DGKε-TG mice were assessed with respect to their susceptibility to hypertrophic response to subpressor doses of subcutaneous phenylephrine administration. No significant changes in body weight, heart rate, and systolic blood pressure were observed between WT and DGKε-TG mice after subcutaneous infusion of phenylephrine as previous studied (1, 20). As shown in Table 1,

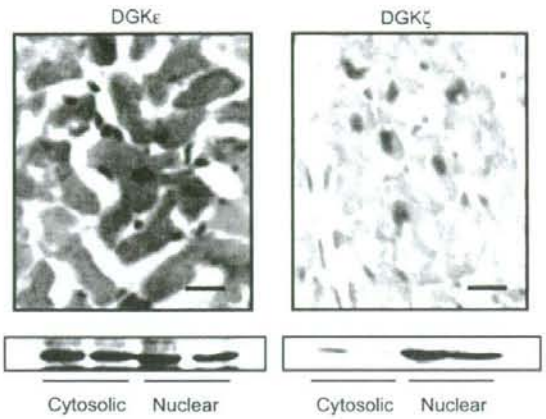

Fig. 2. Immunohistochemical staining and Western blot of left ventricular myocardium of DGKε-TG and DGKζ-TG mice. Bars = 20 μm.

subcutaneous infusion of phenylephrine caused significant increases in the ratio of heart weight to body weight and the ratio of the left ventricular weight to body weight in WT mice. However, these increases were completely blocked in DGKε-TG mice.

We next examined cardiac mRNA expressions of fetal-type genes after phenylephrine infusion. As shown in Table 1, the mRNA expressions of ANF and β-MHC were increased in WT mice given phenylephrine compared with WT mice infused with saline. However, phenylephrine failed to cause gene induction of ANF in DGKε-TG mice.

Effects of DGKε on phenylephrine-induced activation of the DAG-PKC signaling. Lipid extracts were then prepared from the left ventricle, and we quantified myocardial DAG levels in WT and DGKε-TG mouse hearts. As shown in Fig. 3*A*, DAG levels were not different between WT and DGKε-TG mice at the basal condition. In WT mouse hearts, myocardial DAG level increased markedly after continuous administration of phenylephrine. On the other hand, this effect of phenylephrine on myocardial DAG levels was completely suppressed in DGKε-TG mouse hearts.

As shown in Fig. 3*B*, the membrane-associated immunoreactivities of PKCα and -ε were significantly increased in phenylephrine-treated WT mice compared with saline-infused WT mice. However, phenylephrine-induced translocation of PKCα and -ε was significantly attenuated in DGKε-TG mice. The translocation of PKCβ and -δ was not detected after continuous administration of phenylephrine (data not shown). These data suggest that DGKε regulates PKCα and -ε activity by controlling cellular DAG levels.

Cardiac hypertrophy after TAC. Because mechanical stimuli such as pressure and volume overload are clinically relevant and important in cardiac hypertrophy and heart failure, we next examined whether DGKε modifies cardiac remodeling in response to pressure overload using a TAC mouse model (9). Figure 4*A* shows representative transverse sections of WT and DGKε-TG mouse hearts after TAC or sham operation. Extensive cardiac hypertrophy was observed in WT mice at 4 wk after TAC. However, cardiac hypertrophy after TAC was attenuated in DGKε-TG mice. As shown in Table 2, the pressure gradient across the aortic stenosis at 4 wk after TAC surgery was similar between WT and DGKε-TG mice (71 ± 3 vs. 74 ± 4 mmHg). Similarly, the ascending aortic systolic pressure (170 ± 6 vs. 167 ± 7 mmHg) and left ventricular systolic pressure (167 ± 6 vs. 175 ± 9 mmHg) were not different between WT and DGKε-TG mice as in Table 2. These data clearly demonstrated that surgical intervention was equal between WT and DGKε-TG mice. Body weight was not different at 4 wk after TAC, whereas heart weight was markedly increased in WT mice after TAC surgery as reported in Table 2. However, increases in heart weight and left ventricular weight corrected for body weight after TAC were attenuated in DGKε-TG mice compared with WT mice.

Microscopic observations revealed that the cardiomyocyte cross-sectional area was profoundly increased in WT mice at 4 wk after TAC compared with sham-operated WT mice (Fig. 4*B*). However, this increase after TAC was significantly attenuated in DGKε-TG mice compared with WT mice.

DGKε restores cardiac dysfunction under chronic pressure overload. Echocardiography was performed at baseline, 1 wk, and 4 wk after TAC surgery. Under anesthesia, the heart rate was similar between WT and DGKε-TG mice (data not shown). The representative M-mode echocardiograms are shown in Fig. 5, and Table 2 summarizes the echocardiographic data. IVS and PW thickness were significantly increased in WT mice after TAC. However, these increases were significantly attenuated in DGKε-TG mice. Furthermore, the reduction of LVFS and dilatation of LVEDD in

Table 1. *Gravimetric parameters and real-time RT-PCR data in WT and DGKε-TG mice ays after PE infusion*

	WT Saline	DGKε-TG Saline	WT PE	DGKε-TG PE
BW, g	23.0±1.3	21.3±1.6	23.1±0.9	23.2±1.2
SBP, mmHg	104 + 11	103 + 8	107 + 7	111 + 6
HW/BW, mg/g	4.78±0.17	4.98±0.13	6.59±0.32*	4.82±0.15‡
LVW/BW, mg/g	3.17±0.16	3.38±0.09	4.27±0.17*	3.54±0.11‡
RVW/BW, mg/g	0.64±0.07	0.69±0.06	0.78±0.11	0.65±0.03
Lung weight/BW, mg/g	5.94±0.26	6.07±0.16	6.46±0.29	6.47±0.62
Liver weight/BW, mg/g	33.6±1.6	35.4±0.9	36.7±1.7	34.7±1.1
ANF-to-GAPDH ratio, fold increase	1.00±0.08	1.12±0.19	2.52±0.38*	1.28±0.12†
β-MHC-to-GAPDH ratio, fold increase	1.00±0.10	1.22±0.24	2.94±0.79*	1.91±0.23†

Values are means ± SE; $n = 15$ mice. WT, wild-type; DGKε-TG, diacylglycerol kinase-transgenic; PE, phenylephrine; BW, body weight; HW, heart weight; SBP, systolic blood pressure; LVW, left ventricular weight; RVW, right ventricular weight; ANF, atrial natriuretic factor; β-MHC, β-myosin heavy chain; GAPDH, glyceraldehyde-3-phosphate dehydrogenase. *$P < 0.01$ vs. WT-saline mice; †$P < 0.05$ and ‡$P < 0.01$ vs. WT-PE mice.

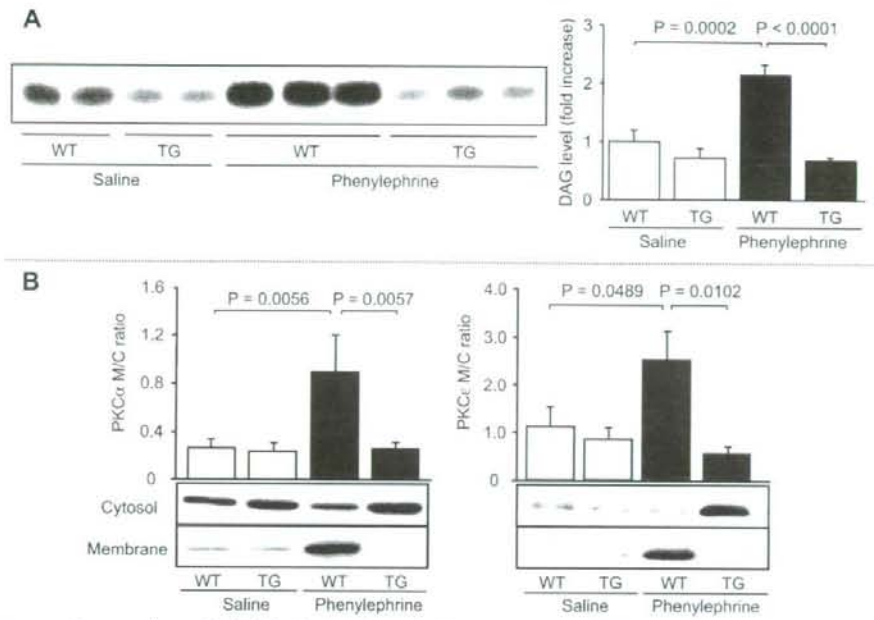

Fig. 3. *A, left*: representative autoradiogram for DAG levels. *A, right*: quantitative data of DAG by scintillation counting. *B*: translocation of PKCα and -ε in WT mice after phenylephrine infusion was abolished in DGKε-TG mice. Data are reported as means ± SE obtained from 8 mice for each group. M/C, membrane-to-cytosol ratio.

WT mice at 4 wk after TAC were prevented in DGKε-TG mice.

Cardiac catheter was performed at baseline and 4 wk after surgery. As shown in Table 2, WT mice after TAC exhibited severe cardiac dysfunction at 4 wk after TAC as demonstrated by increased LVEDP and reduced ±dP/d*t* compared with sham-operated WT mice. However, LVEDP after TAC was significantly reduced in DGKε-TG mice. The ±dP/d*t* after TAC improved in DGKε-TG mice, but these changes were not statistically significant.

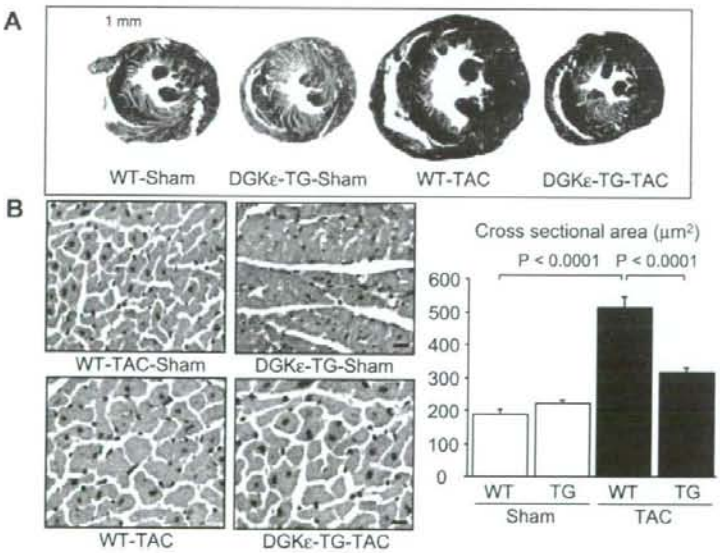

Fig. 4. Histological observations at 4 wk after thoracic transverse aortic constriction (TAC) or sham operation. *A*: representative left ventricular transverse sections stained by hematoxylin-eosin stain. *B, left*: representative images of hematoxylin-eosin micrographs of cardiomyocyte cross sections (magnification, ×400; bar = 20 μm). *B, right*: quantitative analysis of cardiomyocyte cross-sectional area isolated from the left ventricular myocardium. Data are reported as means ± SE obtained from 10–12 mice for each group.

Table 2. *Gravimetric data and cardiac function (echocardiographic and cardiac catheter) at 4 wk after TAC or sham operation*

	WT Sham	DGKε-TG Sham	WT TAC	DGKε-TG TAC
BW, g	23.6±1.0	22.2±1.2	23.8±0.9	22.8±0.9
HW/BW, mg/g	5.19±0.18	5.11±0.23	9.85±0.77†	7.41±0.46§
LVW/BW, mg/g	3.40±0.17	3.33±0.19	6.65±0.37†	5.58±0.24‡
RVW/BW, mg/g	0.70±0.09	0.71±0.07	0.79±0.08	0.61±0.10
Lung weight/BW, mg/g	6.07±0.28	6.18±0.28	11.34±1.71†	7.76±0.71§
Liver weight/BW, mg/g	34.8±1.4	35.9±0.93	38.5±3.0	35.8±1.9
Echocardiographic data				
IVS, mm	0.70±0.02	0.68±0.01	1.10±0.06†	0.78±0.02§
PW, mm	0.71±0.02	0.72±0.03	1.11±0.04*	0.82±0.27‡
LVEDD, mm	3.11±0.03	3.07±0.05	3.36±0.09†	3.08±0.08§
LVFS, %	54.4±1.4	54.4±1.5	34.8±2.8†	43.5±1.0§
LV wall-to-LVEDD ratio	0.47±0.01	0.48±0.01	0.66±0.03†	0.54±0.02§
LVMI/BW, mg/g	2.90±0.17	3.03±0.19	5.31±0.28†	3.48±0.44§
Cardiac catheter data				
HR, beats/min	532±15	555±15	534±10	522±12
Aortic SBP, mmHg	117±6	110±2	170±6†	167±7†
LVSP, mmHg	120±4	109±1	167±6†	175±9†
Pressure gradient, mmHg	2±1	3±1	71±3†	74±4†
LVEDP, mmHg	1.62±0.53	0.81±0.21	12.03±2.12†	5.02±1.88§
+dP/d*t*	13,944±1,166	14,637±1,494	8,647±583*	9,658±1,530
−dP/d*t*	13,941±1,158	14,763±1,866	9,180±746*	11,221±1,059
τ, ms	5.81±0.66	5.46±0.29	5.62±0.40	5.41±0.31

Values are means ± SE; $n = 15$ mice. TAC, thoracic transverse aortic constriction; IVS, interventricular septum; PW, posterior wall; LVESD, left ventricular (LV) end-systolic dimension; LVEDD, LV end-diastolic dimension; LVFS, LV fractional shortening; LV wall, 2 × PW; LVMI, LV mass index; HR, heart rate; LVSP, LV systolic blood pressure; LVEDP, LV end-diastolic pressure; +dP/d*t* and −dP/d*t*, maximal and minimum rates of LV pressure development, respectively; τ, time constant of LV isovolumic relaxation. *$P < 0.05$ and †$P < 0.01$ vs. WT-sham mice; ‡$P < 0.05$ and §$P < 0.01$ vs. WT-TAC mice.

Activation of the DAG-PKC signaling and fetal gene induction after TAC. The DAG level was significantly increased in WT mice at 4 wk after TAC compared with sham-operated WT mice (Fig. 6*A*). On the other hand, the DAG level was completely suppressed in DGKε-TG mice compared with WT mice at 4 wk after TAC.

As shown in Fig. 6*B*, we detected the translocation of PKCα, -β, -δ, and -ε isoforms in WT mice after TAC compared with sham-operated mice. However, in DGKε-TG mice, the translocation of these PKC isoforms after TAC was completely abolished compared with that in the WT mice.

We next examined mRNA expressions of fetal type genes such as ANF, β-MHC, BNP, and α-skeletal actin at 4 wk after surgery. The expressions of ANF, β-MHC, BNP, and α-skeletal actin were significantly upregulated in WT mice after TAC compared with sham-operated WT mice as demonstrated in Table 3. Conversely, in DGKε-TG mice, the gene inductions of ANF, β-MHC, and BNP, but not α-skel-

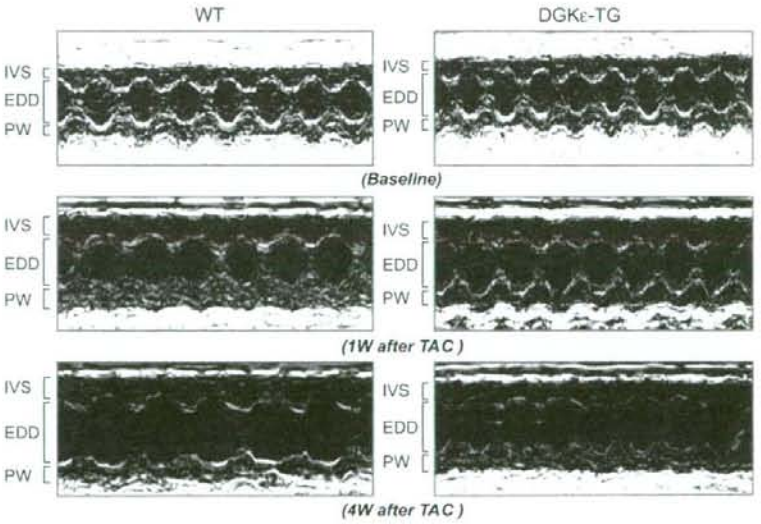

Fig. 5. Representative M-mode echocardiograms at baseline, 1 wk (1w) and 4 wk (4w) after TAC surgery. IVS, interventricular septum; EDD, left ventricular end-diastolic dimension; PW, posterior wall.

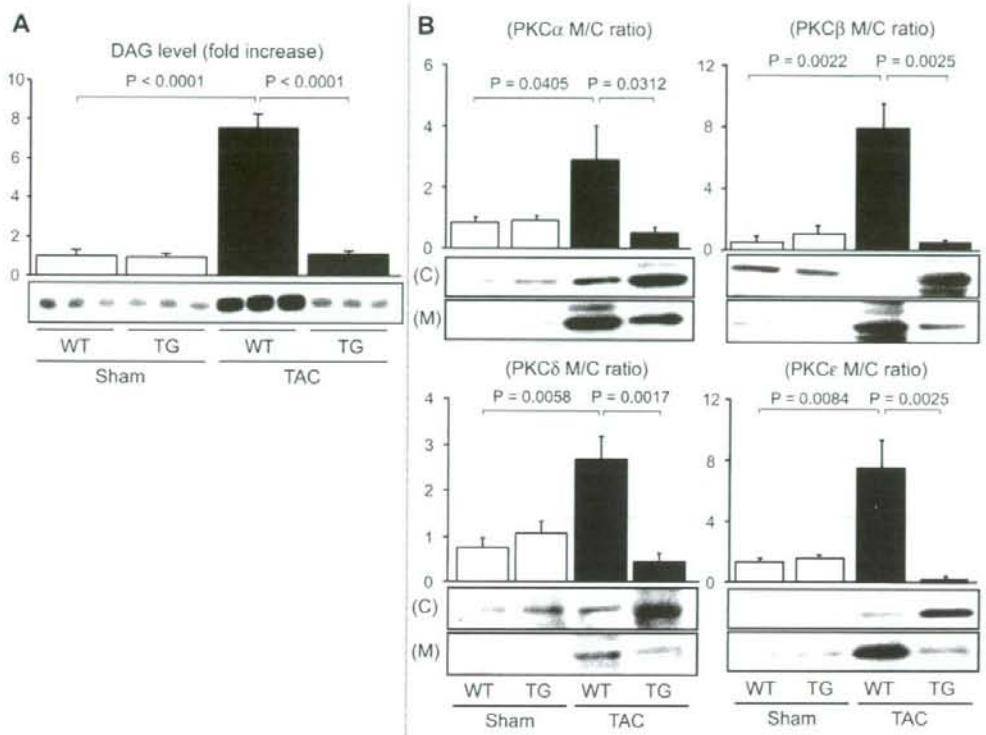

Fig. 6. *A*: increase of DAG level in WT mice at 4 wk after TAC was significantly attenuated in DGKε-TG mice. *B*: translocation of PKCα (*top, left*), -β (*top, right*), -δ (*bottom, left*), and -ε (*bottom, right*) isoforms in WT mice after TAC was significantly attenuated in DGKε-TG mice. Data are reported as means ± SE obtained from 8 mice for each group.

etal actin, were significantly attenuated compared with WT mice.

Myocardial fibrosis and expressions of profibrotic genes after TAC. Since reactive interstitial and perivascular fibrosis adversely alters myocardial stiffness and ultimately leads to left ventricular dysfunction, we examined myocardial fibrosis at 4 wk after surgery using sections stained with Masson's trichrome stain (Fig. 7). Prominent perivascular and interstitial fibrosis was observed in WT mice after TAC as reported in previous studies (9). However, the degree of myocardial fibro-

Table 3. *Fetal type genes, profibrotic genes, and TRPC isoform expressions by real-time RT-PCR analysis at 4 wk after TAC or sham operation*

	WT Sham	DGKε-TG Sham	WT TAC	DGKε-TG TAC
Fetal type genes				
ANF-to-GAPDH ratio, fold increase	1.00±0.23	0.98±0.30	3.30±1.24†	1.05±0.64‡
β-MHC-to-GAPDH ratio, fold increase	1.00±0.57	0.74±0.33	6.65±2.23*	3.13±1.12‡
BNP-to-GAPDH ratio, fold increase	1.00±0.11	0.87±0.35	8.14±2.49†	2.86±1.29‡
α-Skeletal actin-to-GAPDH ratio, fold increase	1.00±0.32	0.85±0.16	10.04±3.18†	8.78±3.77†
Profibrotic genes				
Collagen type I-to-GAPDH ratio, fold increase	1.00±0.22	0.88±0.17	1.63±0.11*	0.82±0.09§
Collagen type III-to-GAPDH ratio, fold increase	1.00±0.11	0.85±0.28	2.69±0.43†	0.76±0.09§
Collagen type I-to-type III ratio	1.00 + 0.90	0.73 + 0.18	2.32 + 1.40†	0.66 + 0.17§
TRPC isoforms				
TRPC 1-to-GAPDH ratio, fold increase	1.00±0.16	1.16±0.47	1.07±0.21	0.70±0.21
TRPC 3-to-GAPDH ratio, fold increase	1.00±0.20	1.40±0.33	1.38±0.25	1.61±0.40
TRPC 4-to-GAPDH ratio, fold increase	1.00±0.20	1.70±0.54	1.35±0.24	1.19±0.20
TRPC 6-to-GAPDH ratio, fold increase	1.00±0.18	1.44±0.58	3.23±0.41†	1.52±0.43§

Values are means ± SE; $n = 15$ mice. BNP, brain natriuretic peptide; TRPC, transient receptor potential channel. *$P < 0.05$ and †$P < 0.01$ vs. WT-Sham mice; ‡$P < 0.05$ and §$P < 0.01$ vs. WT-TAC mice.

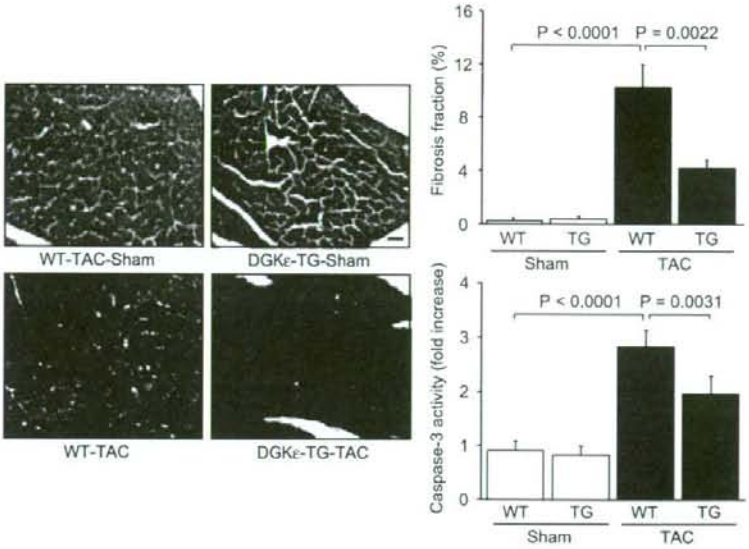

Fig. 7. Histological analyses at 4 wk after surgery. *Left*: representative images of Masson's trichrome stain (Magnification, ×400; bar = 20 μm) in the left ventricular myocardium. *Right, top*: comparison of the fibrosis fraction. *Right, bottom*: comparison of caspase-3 activity. Data are reported as means ± SE obtained from 8 mice for each group.

sis after TAC was much less in DGKε-TG mice than in WT mice as shown in Fig. 7. Furthermore, although caspase-3 activity associated with fibrosis was significantly increased in WT mice after TAC as previous studied (23), this increase was attenuated in DGKε-TG mice.

We next examined the expressions of profibrotic genes such as collagen types I and III to investigate whether these morphological observations were accompanied by alterations in gene expressions relevant to fibrotic changes. Real-time RT-PCR revealed that collagen types I and III mRNA and the ratio of collagen type I to type III were markedly upregulated in WT mice at 4 wk after TAC compared with sham-operated WT mice (Table 3). However, these responses after TAC were significantly attenuated in DGKε-TG mice compared with WT mice.

TRPC isoform expressions after TAC surgery by real-time RT-PCR and Western blot analysis. Recently, it has been reported that a DAG-mediated increase in cytosolic Ca^{2+} via TRPC participates in a positive regulatory circuit in the calcineurin-nuclear factor of activated T cells (NFAT) pathway leading to pathological cardiac hypertrophy (15). Since DAG produced by PLC activation directly activates TRPC 6 (19), we next examined TRPC isoform expressions in WT and DGKε-TG mice at 4 wk after TAC surgery.

We detected cardiac expressions of TRPC 1, 3, 4 and 6, and only TRPC-6 expression was significantly upregulated in WT mice at 4 wk after TAC by both real-time RT-PCR analysis (Table 3) and Western blot analysis (Fig. 8). However, in DGKε-TG mice, this upregulation of TRPC 6 after TAC was significantly attenuated compared with WT mice.

DGKε improves survival after TAC. As shown in Fig. 9, the Kaplan-Meier survival curves were created from 38 TAC-operated WT mice, 31 TAC-operated DGKε-TG mice, 14 sham-operated WT mice, and 15 sham-operated DGKε-TG mice. Some TAC mice died suddenly, and an autopsy revealed that those mice had enlarged hearts with severe myocardial fibrosis accompanied by pericardial and pleural effusion. The survival rate in TAC-operated WT mice was 42.8% at 4 wk after surgery. However, cardiac DGKε expression improved the survival rate after TAC to 79.2% ($P = 0.0334$). Furthermore, the presence of a pleural effusion was less in DGKε-TG mice compared with WT mice at 4 wk after TAC [5/31 (16%) vs. 17/38 (45%), $P = 0.0345$]. Thus these observed differences in survival rate might be due to less lethal congestive heart failure in DGKε-TG mice than in WT mice.

DISCUSSION

This is the first report characterizing a functional role of DGKε in in vivo mouse hearts. We demonstrated that DGKε blocks the hypertrophic signaling cascade and the resultant cardiac hypertrophy in response to phenylephrine infusion and chronic pressure overload. We showed that cardiac fibrosis, an increase of myocardial DAG level, the translocation of PKC isoforms, caspase-3 activity, the induction of fetal and profibrotic genes, and the upregulation of TRPC 6 in WT mice after TAC were significantly blocked by DGKε. Furthermore, DGKε prevented the progression to heart failure after TAC without detectable adverse effects in in vivo hearts. The fact that controlling the GPCR signaling pathway by DGKε prevents developing heart failure after TAC suggests that DGKε may represent a novel therapeutic target for cardiac hypertrophy and the progression to subsequent heart failure.

Numerous investigations have demonstrated the importance of $G\alpha_q$-mediated signaling in the development of cardiac hypertrophy (6, 11). We have previously shown that DGKζ inhibits GPCR agonist-induced hypertrophic signaling pathway and the resultant cardiac hypertrophy in vitro and in vivo (1, 28). On the other hand, previous reports suggest that DGK isoforms have different functional roles and substrate specificity in signal transduction pathway (22, 29, 38). In infarcted rat hearts, the DGKζ expression was enhanced in the infarcted

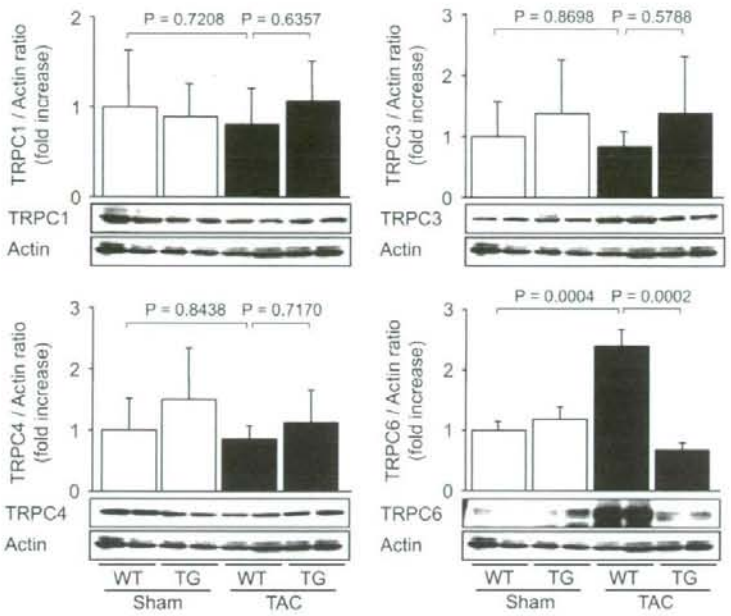

Fig. 8. Expressions of transient receptor potential channel (TRPC) isoforms at 4 wk after TAC or sham operation. Data of TRPC were normalized by actin. Upregulation of TRPC 6 detected in WT mice after TAC was significantly attenuated in DGKε-TG mice. Data are reported as means ± SE obtained from 8 mice for each group.

area and border zone (29). In contrast, the DGKε expression was decreased in viable myocardium and was completely restored by treatment with captopril. No significant difference in the expression of DGKζ was observed in left ventricular myocardium between TAC-operated and sham-operated rats at 3, 7, and 28 days after surgery (38). However, the DGKε expression in left ventricular myocardium was significantly decreased after TAC. Furthermore, the overexpressing DGKε especially reduced the polyunsaturated DAG levels and caused the redistribution of PKCα and -ε isoforms in porcine aortic endothelial cells (22), whereas the overexpression of DGKζ caused very little changes in DAG levels and PKC distribution. In contrast to DGKζ (1, 28), DGKε inhibited the translocation of PKCβ and -δ after TAC in the present study. In addition, DGKε completely blocked phenylephrine-induced cardiac hypertrophy (Table 1). Since the localization of the enzymes has a marked impact on signaling cascade (36), these results might be due to substrate specificity toward arachidonoyl-containing DAG in DGKε (22) and differences in subcellular localization (14), DGKζ in the nucleus, and DGKε in cytoplasm and nucleus (Fig. 2). Because the DAG-binding site in DGK has not yet been identified with certainty, this needs to be further examined in the future. Since this study employed only the overexpression approach, future experiments of a loss of DGK function using knockout mice are necessary to elucidate further the role of DGKε in signaling cascade in vivo.

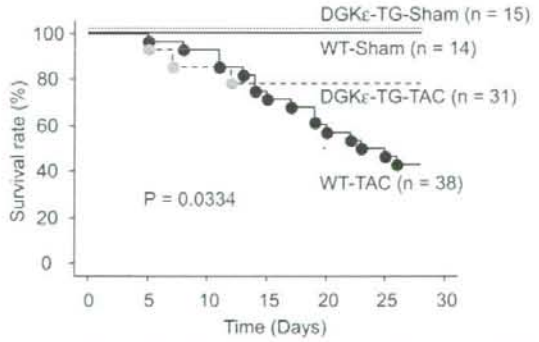

Fig. 9. Survival curves in WT and DGKε-TG mice after TAC or sham operation. Percentages of surviving WT and DGKε-TG mice were plotted. During follow-up period, survival rates after TAC were significantly higher in DGKε-TG mice than in WT mice. *n*, Number of mice.

The systolic blood pressure after the infusion of phenylephrine was not different among DGKε-TG and WT mice, indicating that the overexpression of DGKε does not affect hemodynamic regulations in response to phenylephrine. Thus the hypertrophic response in this phenylephrine model occurred independently of the hemodynamic effects of phenylephrine because the systemic blood pressure was not elevated after the infusion. The dose of phenylephrine used in this study (20 $mg \cdot kg^{-1} \cdot day^{-1}$) was lower compared with the dose (100 $mg \cdot kg^{-1} \cdot day^{-1}$) of the other study (13).

In this study, the DAG level was significantly increased in WT mice at 4 wk after TAC compared with sham-operated WT mice. However, this increase was significantly attenuated in DGKε-TG mice. Wang et al. (35) reported that PLC activity was substantially increased in WT mice at 6 wk after TAC compared with sham-operated mice. Both PLC activity and reduction in DAG clearance might influence myocardial DAG levels and explain the effectiveness of DGKε.

TRPC is one of the candidate channel subunits responsible for receptor-activated Ca^{2+} entry and store-operated Ca^{2+} entry. Cytoplasmic free Ca^{2+} in cardiomyocytes induces pos-

itive inotropic effects on the heart and activates several transcriptional pathways, such as NFAT signaling, that lead to cardiac hypertrophy. Recent reports have demonstrated that TRPC 6 is activated directly by DAG and stretch stimuli and that TRPC 6 is involved in NFAT activation during pathological cardiac remodeling in in vivo hearts (19, 27). Furthermore, it has been reported that TRPC 6 expression was upregulated in mouse hearts expressing constitutively active calcineurin and subjected to pressure overload by TAC (15) and the infusion of phenylephrine and endothelin-1 (5), because the promoter of the TRPC 6 gene contains two conserved NFAT-binding sites that confer responsiveness to calcineurin-NFAT signaling translationally. The overexpression of TRPC 6 in cardiomyocytes activates the NFAT and increases in the expression of β-MHC (15). Furthermore, small-interfering RNA knockdown of TRPC 6 reduces hypertrophic signaling by phenylephrine and endothelin-1, suggesting that TRPC 6 participates in a positive regulatory circuit in the calcineurin-NFAT pathway in response to GPCR signaling (15). We demonstrated for the first time that DAG-mediated expression of TRPC 6 after TAC was blocked by DGKε in this study. The attenuation of DAG signaling by DGKε might inhibit TRPC-6 expression by the regulation of calcineurin-NFAT signaling. Although we were unable to measure TRPC-6 activity, the altered DAG metabolism may impact on the posttranslational regulation of TRPC activity. These data suggest that TRPC might contribute to cardiac hypertrophy and the progression to heart failure under chronic pressure overload.

Previous studies have reported that the PKCδ and -ε isoforms play an important role in cardiac hypertrophy (4, 32). The PKCε activates ERK-AP-1 signaling pathway, leading to myocardial hypertrophy and increases in protein synthesis (28). It has been reported that PKCβ plays a critical role in the development of heart failure (30) and that PKCα induces reactive fibrosis, impairing both systolic and diastolic function and leading to early heart failure and premature lethality (8). Furthermore, the GPCR agonist activates c-jun NH_2-terminal kinase and p38 mitogen-activated protein kinase through PLC-PKC pathways in the cardiomyocyte, and these pathways act as potent signals for cardiac hypertrophy and the progression to heart failure (24). Thus the inhibition of PKC translocation by DGKε in this study might attenuate cardiac hypertrophy and fibrosis and prevent progression to heart failure after TAC. Membrane and cytosolic Western blot analysis for PKC suggested that the transcriptional activation of PKC protein synthesis upon TAC had occurred to coordinate the increase of protein in the course of hypertrophic development as previously studied (4, 12).

DGKε-TG mice showed a complete inhibition of hypertrophy in response to phenylephrine but only a partial inhibition of the hypertrophic response to TAC. Because the cardiac hypertrophy caused by TAC was induced by various signaling pathways such as gp130-STAT3 (34), G_q protein-coupled receptor-adenylyl cyclase signaling pathway (10), and glycogen synthase kinase-3 (39), DGKε could not inhibit hypertrophy after TAC completely. In this study the survival rate after TAC was lower compared with that in other reports (2, 21). Because other studies used C57BL6/J (2) and FVB mice (21), the difference of background might contribute to the survival rate in this study. The cause of death was considered due to congestive heart failure with the following signs: the presence of pulmonary congestion (increased lung weight) and massive chest fluid accumulation as described previously (18). Future studies are needed to examine survival rate after longer periods of TAC between DGKε-TG and WT mice.

Conclusions. We demonstrated that DGKε is a new specific regulator of GPCR signaling in cardiomyocytes. DGKε inhibits the activation of PKC and the expression of TRPC by controlling cellular DAG levels. These results will allow us a novel approach to investigate the pathogenesis of cardiac hypertrophy and heart failure, and DGKε may be a potential novel therapeutic target to prevent heart failure.

GRANTS

This study was supported in part by the Ministry of Education, Science, Sports and Culture, Japan, Grant-in-Aid for Scientific Research No. 19590804.

REFERENCES

1. **Arimoto T, Takeishi Y, Takahashi H, Shishido T, Niizeki T, Koyama Y, Shiga R, Nozaki N, Nakajima O, Nishimaru K, Abe J, Endoh M, Walsh RA, Goto K, Kubota I.** Cardiac-specific overexpression of diacylglycerol kinase zeta prevents Gq protein-coupled receptor agonist-induced cardiac hypertrophy in transgenic mice. *Circulation* 113: 60–66, 2006.
2. **Asaumi Y, Kagaya Y, Takeda M, Yamaguchi N, Tada H, Ito K, Ohta J, Shiroto T, Shirato K, Minegishi N, Shimokawa H.** Protective role of endogenous erythropoietin system in nonhematopoietic cells against pressure overload-induced left ventricular dysfunction in mice. *Circulation* 115: 2022–2032, 2007.
3. **Bowling N, Walsh RA, Song G, Estridge T, Sandusky GE, Fouts RL, Mintze K, Pickard T, Roden R, Bristow MR, Sabbah HN, Mizrahi JL, Gromo G, King GL, Vlahos CJ.** Increased protein kinase C activity and expression of Ca^{2+}-sensitive isoforms in the failing human heart. *Circulation* 99: 384–391, 1999.
4. **Braun MU, LaRosée P, Schön S, Borst MM, Strasser RH.** Differential regulation of cardiac protein kinase C isozyme expression after aortic banding in rat. *Cardiovasc Res* 56: 52–63, 2002.
5. **Bush EW, Hood DB, Papst PJ, Chapo JA, Minobe W, Bristow MR, Olson EN, McKinsey TA.** Canonical transient receptor potential channels promote cardiomyocyte hypertrophy through activation of calcineurin signaling. *J Biol Chem* 281: 33487–33496, 2006.
6. **Dorn GW 2nd, Brown JH.** Gq signaling in cardiac adaptation and maladaptation. *Trends Cardiovasc Med* 9: 26–34, 1999.
7. **Goto K, Kondo H.** A 104-kDa diacylglycerol kinase containing ankyrin-like repeats localizes in the cell nucleus. *Proc Natl Acad Sci USA* 93: 11196–11201, 1996.
8. **Hahn HS, Marreez Y, Odley A, Sterbling A, Yussman MG, Hilty KC, Bodi I, Liggett SB, Schwartz A, Dorn GW 2nd.** Protein kinase Calpha negatively regulates systolic and diastolic function in pathological hypertrophy. *Circ Res* 93: 1111–1119, 2003.
9. **Harada M, Takeishi Y, Arimoto T, Niizeki T, Kitahara T, Goto K, Walsh RA, Kubota I.** Diacylglycerol kinase zeta attenuates pressure overload-induced cardiac hypertrophy. *Circ J* 71: 276–282, 2007.
10. **Holmer SR, Bruckschlegel G, Schunkert H, Rataj DB, Kromer EP, Riegger GA.** Functional activity and expression of the myocardial postreceptor adenylyl cyclase system in pressure overload hypertrophy in rat. *Cardiovasc Res* 31: 719–728, 1996.
11. **Hunter JJ, Chien KR.** Signaling pathways for cardiac hypertrophy and failure. *N Engl J Med* 341: 1276–1283, 1999.
12. **Jalili T, Takeishi Y, Song G, Ball NA, Howles G, Walsh RA.** PKC translocation without changes in Galphaq and PLC-β protein abundance in cardiac hypertrophy and failure. *Am J Physiol Heart Circ Physiol* 277: H2298–H2304, 1999.
13. **Keys JR, Greene EA, Koch WJ, Eckhart AD.** Gq-coupled receptor agonists mediate cardiac hypertrophy via the vasculature. *Hypertension* 40: 660–666, 2002.
14. **Kobayashi N, Hozumi Y, Ito T, Hosoya T, Kondo H, Goto K.** Differential subcellular targeting and activity-dependent subcellular localization of diacylglycerol kinase isozymes in transfected cells. *Eur J Cell Biol* 86: 433–444, 2007.

15. **Kuwahara K, Wang Y, McAnally J, Richardson JA, Bassel-Duby R, Hill JA, Olson EN.** TRPC6 fulfills a calcineurin signaling circuit during pathologic cardiac remodeling. *J Clin Invest* 116: 3114–3126, 2006.
16. **Levy D, Garrison RJ, Savage DD, Kannel WB, Castelli WP.** Prognostic implications of echocardiographically determined left ventricular mass in the Framingham Heart Study. *N Engl J Med* 322: 1561–1566, 1990.
17. **Mende U, Kagen A, Cohen A, Aramburu J, Schoen FJ, Neer EJ.** Transient cardiac expression of constitutively active Galphaq leads to hypertrophy and dilated cardiomyopathy by calcineurin-dependent and independent pathways. *Proc Natl Acad Sci USA* 95: 13893–13898, 1998.
18. **Niizeki T, Takeishi Y, Arimoto T, Takahashi H, Shishido T, Koyama Y, Goto K, Walsh RA, Kubota I.** Cardiac-specific overexpression of diacylglycerol kinase ζ attenuates left ventricular remodeling and improves survival after myocardial infarction. *Am J Physiol Heart Circ Physiol* 292: H1105–H1112, 2007.
19. **Onohara N, Nishida M, Inoue R, Kobayashi H, Sumimoto H, Sato Y, Mori Y, Nagao T, Kurose H.** TRPC3 and TRPC6 are essential for angiotensin II-induced cardiac hypertrophy. *EMBO J* 25: 5305–5316, 2006.
20. **Otani H, Otani H, Das DK.** Alpha 1-adrenoceptor-mediated phosphoinositide breakdown and inotropic response in rat left ventricular papillary muscles. *Circ Res* 62: 8–17, 1998.
21. **Ovechkin AV, Tyagi N, Rodriguez WE, Hayden MR, Moshal KS, Tyagi SC.** Role of matrix metalloproteinase-9 in endothelial apoptosis in chronic heart failure in mice. *J Appl Physiol* 99: 2398–2405, 2005.
22. **Pettitt TR, Wakelam MJ.** Diacylglycerol kinase epsilon, but not zeta, selectively removes polyunsaturated diacylglycerol, inducing altered protein kinase C distribution in vivo. *J Biol Chem* 274: 36181–38186, 1999.
23. **Philipp S, Pagel I, Höhnel K, Lutz J, Buttgereit J, Langenickel T, Hamet P, Dietz R, Willenbrock R.** Regulation of caspase 3 and Fas in pressure overload-induced left ventricular dysfunction. *Eur J Heart Fail* 6: 845–851, 2004.
24. **Sabri A, Wilson BA, Steinberg SF.** Dual actions of the Galpha(q) agonist *Pasteurella multocida* toxin to promote cardiomyocyte hypertrophy and enhance apoptosis susceptibility. *Circ Res* 90: 850–857, 2002.
25. **Sadoshima J, Izumo S.** Signal transduction pathways of angiotensin II-induced c-fos gene expression in cardiac myocytes in vitro. Roles of phospholipid-derived second messengers. *Circ Res* 73: 424–438, 1993.
26. **Shubeita HE, McDonough PM, Harris AN, Knowlton KU, Glembotski CC, Brown JH, Chien KR.** Endothelin induction of inositol phospholipid hydrolysis, sarcomere assembly, and cardiac gene expression in ventricular myocytes. A paracrine mechanism for myocardial cell hypertrophy. *J Biol Chem* 265: 20555–20562, 1990.
27. **Spassova MA, Hewavitharana T, Xu W, Soboloff J, Gill DL.** A common mechanism underlies stretch activation and receptor activation of TRPC6 channels. *Proc Natl Acad Sci USA* 103: 16586–16591, 2006.
28. **Takahashi H, Takeishi Y, Seidler T, Arimoto T, Akiyama H, Hozumi Y, Koyama Y, Shishido T, Tsunoda Y, Niizeki T, Nozaki N, Abe J, Hasenfuss G, Goto K, Kubota I.** Adenovirus-mediated overexpression of diacylglycerol kinase-zeta inhibits endothelin-1-induced cardiomyocyte hypertrophy. *Circulation* 111: 1510–1516, 2005.
29. **Takeda M, Kagaya Y, Takahashi J, Sugie T, Ohta J, Watanabe J, Shirato K, Kondo H, Goto K.** Gene expression and in situ localization of diacylglycerol kinase isozymes in normal and infarcted rat hearts: effects of captopril treatment. *Circ Res* 89: 265–272, 2001.
30. **Takeishi Y, Chu G, Kirkpatrick DM, Li Z, Wakasaki H, Kranias EG, King GL, Walsh RA.** In vivo phosphorylation of cardiac troponin I by protein kinase Cbeta2 decreases cardiomyocyte calcium responsiveness and contractility in transgenic mouse hearts. *J Clin Invest* 102: 72–78, 1998.
31. **Takeishi Y, Jalili T, Ball NA, Walsh RA.** Responses of cardiac protein kinase C isoforms to distinct pathological stimuli are differentially regulated. *Circ Res* 85: 264–271, 1999.
32. **Takeishi Y, Ping P, Bolli R, Kirkpatrick DL, Hoit BD, Walsh RA.** Transgenic overexpression of constitutively active protein kinase C epsilon causes concentric cardiac hypertrophy. *Circ Res* 86: 1218–1223, 2000.
33. **Topham MK, Prescott SM.** Mammalian diacylglycerol kinases, a family of lipid kinases with signaling functions. *J Biol Chem* 274: 11447–11450, 1999.
34. **Uozumi H, Hiroi Y, Zou Y, Takimoto E, Toko H, Niu P, Shimoyama M, Yazaki Y, Nagai R, Komuro I.** gp130 plays a critical role in pressure overload-induced cardiac hypertrophy. *J Biol Chem* 276: 23115–23119, 2001.
35. **Wang BH, Du XJ, Autelitano DJ, Milano CA, Woodcock EA.** Adverse effects of constitutively active α_{1B}-adrenergic receptors after pressure overload in mouse hearts. *Am J Physiol Heart Circ Physiol* 279: H1079–H1086, 2000.
36. **Wattenberg BW, Pitson SM, Raben DM.** The sphingosine and diacylglycerol kinase superfamily of signaling kinases: localization as a key to signaling function. *J Lipid Res* 47: 1128–1139, 2006.
37. **Weiss JL, Frederiksen JW, Weisfeldt ML.** Hemodynamic determinants of the time-course of fall in canine left ventricular pressure. *J Clin Invest* 58: 751–760, 1976.
38. **Yahagi H, Takeda M, Asaumi Y, Okumura K, Takahashi R, Takahashi J, Ohta J, Tada H, Minatoya Y, Sakuma M, Watanabe J, Goto K, Shirato K, Kagaya Y.** Differential regulation of diacylglycerol kinase isozymes in cardiac hypertrophy. *Biochem Biophys Res Commun* 332: 101–108, 2005.
39. **Zhai P, Gao S, Holle E, Yu X, Yatani A, Wagner T, Sadoshima J.** Glycogen synthase kinase-3alpha reduces cardiac growth and pressure overload-induced cardiac hypertrophy by inhibition of extracellular signal-regulated kinases. *J Biol Chem* 282: 33181–33191, 2007.
40. **Zhai P, Yamamoto M, Galeotti J, Liu J, Masurekar M, Thaisz J, Irie K, Holle E, Yu X, Kupershmidt S, Roden DM, Wagner T, Yatani A, Vatner DE, Vatner SF, Sadoshima J.** Cardiac-specific overexpression of AT_1 receptor mutant lacking G alpha q/G alpha i coupling causes hypertrophy and bradycardia in transgenic mice. *J Clin Invest* 115: 3045–3056, 2005.

IJCA-11395; No of Pages 3

ELSEVIER

International Journal of Cardiology xx (2008) xxx – xxx

International Journal of Cardiology

www.elsevier.com/locate/ijcard

Letter to the Editor

Synergistic effect of dual chamber pacing and disopyramide in obstructive hypertrophic cardiomyopathy

Yuichiro Minami [a], Katsuya Kajimoto [a,*], Masatoshi Kawana [a], Nobuhisa Hagiwara [a], Mark V. Sherrid [b]

[a] *Department of Cardiology, Tokyo Women's Medical University, Tokyo, Japan*
[b] *Division of Cardiology, St. Luke's-Roosevelt Hospital Center, College of Physicians and Surgeons, Columbia University, New York, NY, U.S.A.*

Received 8 November 2008; accepted 15 November 2008

Abstract

This study examines acute effect of dual-chamber (DDD) pacing combined with disopyramide for left ventricular outflow tract (LVOT) gradient reduction in obstructive hypertrophic cardiomyopathy (HCM) patients. Among 24 patients refractory to maximal drug therapy, 7 had a significant improvement of LVOT gradient by DDD pacing alone. In the remaining 17 patients, the LVOT gradient reduction was 26±19% after DDD pacing alone and 35±16% after intravenous disopyramide alone. In contrast, after the combined therapy of DDD pacing and disopyramide, pressure gradient decreased from 102±35 to 28±23 mm Hg, a reduction of 72±21%. We have demonstrated synergy between DDD pacing and disopyramide for LVOT gradient reduction in obstructive HCM. Study of the long-term effects of this combined therapy would be the next step to ascertain clinical utility.

Keywords: Hypertrophic cardiomyopathy; Dual chamber pacing; Disopyramide

1. Introduction

Left ventricular outflow tract (LVOT) gradient occurs at rest in roughly 25% of patients with hypertrophic cardiomyopathy (HCM), and is an independent predictor of adverse clinical consequences [1]. This study was undertaken to examine the effect of combined therapy of disopyramide with dual-chamber (DDD) pacing for LVOT gradient reduction in a group of obstructed HCM patients refractory to medical therapy.

2. Methods

A total of 484 consecutive patients with HCM were assessed, between November 1980 and August 2005. The diagnosis of HCM was based on the identification by two-dimensional echocardiography of a hypertrophied, non-dilated left ventricle in the absence of another disease capable of producing a similar degree of hypertrophy. Among these 484 patients, 109 patients had a significant LVOT gradient at rest (≥30 mm Hg) with the use of continuous-wave Doppler echocardiography. Forty-two of 109 obstructive HCM patients had severe symptoms (NYHA III or IV) unresponsive to maximal medications. Among these 42 patients, 18 patients were referred for clinical indications to surgical septal myectomy and permanent DDD pacemaker implantation without temporary DDD pacing study; these patients were excluded. Therefore, the study group consisted of the remaining 24 patients with obstructive HCM. The present study was conducted in accordance with the Declaration of Helsinki and all the patients gave a written informed consent after receiving a written explanation.

Catheterization was performed in the fasting state, and all cardiac medications were withheld 48 h prior to the procedure.

* Corresponding author. Department of Cardiology, Tokyo Women's Medical University, 8-1, Kawada-cho, Shinjuku-ku, Tokyo, 162-8666, Japan. Tel.: +81 3 3353 8111; fax: +81 3 3356 0441.
E-mail address: kkajimoto@comet.ocn.ne.jp (K. Kajimoto).

0167-5273/$ - see front matter © 2008 Elsevier Ireland Ltd. All rights reserved.
doi:10.1016/j.ijcard.2008.11.088

Please cite this article as: Minami Y, et al, Synergistic effect of dual chamber pacing and disopyramide in obstructive hypertrophic cardiomyopathy, Int J Cardiol (2008), doi:10.1016/j.ijcard.2008.11.088

Table 1
Baseline characteristics of the overall study obstructive HCM patients, and responders and non-responders for DDD pacing study

	All patients	Effects of DDD pacing study		
		Responders	Non-responders	p value
No.	24	7	17	
Male/female	12/12	4/3	8/9	$p=0.67$
Age at initial HCM diagnosis, years	52±16	49±15	54±16	$p=0.46$
Age at DDD pacing study, years	56±15	54±13	57±16	$p=0.67$
LVOT gradient at baseline, mm Hg	89±38	58±20	102±35	$p=0.005$
% Reduction in gradient after DDD pacing, %	38±27	68±18	26±19	$p<0.0001$
Mean heart rate during DDD pacing, /min	77±11	74±14	78±9	$p=0.49$
Mean atrioventricular interval, ms	77±30	74±15	78±25	$p=0.78$
Medications				
Beta-blockers	22(92%)	6(86%)	16(94%)	$p=0.52$
Type I antiarrhythmic drugs	20(83%)	6(86%)	14(82%)	$p=0.85$
Calcium channel blockers	8(33%)	2(29%)	6(35%)	$p=0.76$
Amiodarone	3(13%)	1(14%)	2(12%)	$p=0.87$
Symptomatic presentation				
Dyspnea	17(71%)	5(71%)	12(71%)	$p=0.97$
Chest pain	5(21%)	1(14%)	4(24%)	$p=0.63$
Syncope	4(17%)	2(29%)	2(12%)	$p=0.34$
Arrhythmia				
Atrial fibrillation	8(33%)	1(14%)	7(41%)	$p=0.22$
Non-sustained ventricular tachycardia	6(25%)	3(43%)	3(18%)	$p=0.21$

DDD = dual-chamber; HCM = hypertrophic cardiomyopathy; LVOT = left ventricular outflow tract.
Values are given as mean ± SD or n (%).

Pressure tracings at the left ventricular apex and aorta were recorded simultaneously using a fluid-filled system. Temporary DDD pacing study was performed with catheter electrodes positioned at the right atrium and right ventricular apex. Pacing study was then performed with atrial (AAI) pacing and DDD mode, at atrioventricular intervals of 50, 100, or 150 ms. The optimal atrioventricular interval was defined as that producing the lowest LVOT gradient without compromise of aortic pressure. Also, complete right ventricular pre-excitation, as assessed by the QRS morphology, was required to achieve the optimal hemodynamic benefit. The acute efficacy of DDD pacing was defined as a significant reduction of LVOT gradient: LVOT gradient <30 mm Hg or a LVOT gradient reduction >50% after therapy. In patients who failed to have a significant improvement of LVOT gradient by DDD pacing alone, we then administered intravenous disopyramide (1.0 mg/kg). After assessing gradient reduction with intravenous disopyramide, we then reinstituted DDD pacing at optimal atrioventricular delay to assess the combined effect on gradient.

Data were presented as mean ± SD. Student's t test was used to compare two groups for continuous variables. Fisher's exact probability method was used to compare categorical variables. Dunnet multiple comparison method was applied for repeated measures data. Two-tailed p values of less than 0.05 were considered to indicate a statistically significant difference.

3. Results

The clinical and demographic characteristics of the overall study population, and responders and non-responders for DDD pacing study are shown in Table 1. Among 24 patients, 7 patients had a significant improvement of LVOT gradient by DDD pacing alone. Therefore, in the remaining 17 patients, we compared combined therapy of temporary DDD pacing and disopyramide to either therapy alone. In these 17 patients, the LVOT gradient reduction was 26±19% after DDD pacing alone and 35±16% after intravenous disopyramide alone. In contrast, after the combined therapy of temporary DDD pacing and disopyramide, gradient decreased from 102±35 to 28±23 mm Hg ($p<0.05$), a reduction of 72±21% ($p<0.05$ compared with the reduction from disopyramide alone, and $p<0.05$ compared with the reduction from DDD pacing alone; Fig. 1). Fifteen of 17 patients (88%) had a marked and

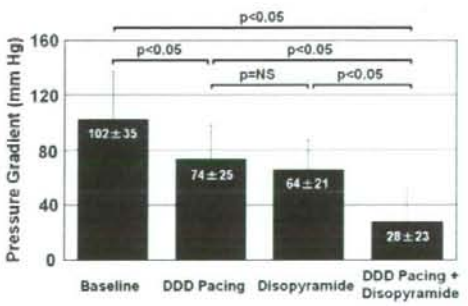

Fig. 1. Change of LVOT gradient with DDD pacing, administration of disopyramide, and a combined therapy of DDD pacing and disopyramide. p values were obtained by Dunnet multiple comparison method. DDD = dual-chamber; LVOT = left ventricular outflow tract.

Please cite this article as: Minami Y, et al, Synergistic effect of dual chamber pacing and disopyramide in obstructive hypertrophic cardiomyopathy. Int J Cardiol (2008), doi:10.1016/j.ijcard.2008.11.088

significant improvement of gradient with combined therapy. Overall, 22 of the 24 patients (92%) had LVOT gradient <30 mm Hg or a gradient reduction >50% with temporary DDD pacing alone therapy ($N=7$) or the combined therapy ($N=15$).

4. Discussion

In this study, we have demonstrated synergy between DDD pacing and disopyramide for gradient reduction in obstructive HCM, during acute testing in the catheterization laboratory. Disopyramide is a potent negative inotrope, and previously has been shown to decrease gradients acutely and long term, with a parallel improvement in symptoms and exercise tolerance [2–5]. Two-thirds of patients who would otherwise need septal reduction therapy were successfully managed medically by the combination of disopyramide and beta-blockers after >3 years [5]. DDD pacing has been previously shown to decrease gradients acutely and chronically [6–9]. While cohort studies suggested that DDD pacing reduced LVOT gradient and symptoms, randomized blinded cross-over studies showed less impressive improvement of gradient and quality of life [7–9]. Therefore, pacing is currently not viewed as applicable as a primary therapy for all obstructive HCM patients [10].

Although pharmacologic agents are the first line of therapy for the relief of LVOT gradient, a subgroup of patients is refractory to pharmacologic therapy or may not tolerate it. Surgical septal myectomy has been employed with considerable success for over 40 years and is considered the gold-standard of treatment for drug refractory patients [10]. However, myectomy requires sternotomy and cardiopulmonary bypass and may be associated with morbidity and mortality. Alcohol septal ablation has also been widely adopted, but it is not as effective as myectomy for reducing gradient or symptoms [11]. Recently, widespread use of alcohol ablation in young patients has been questioned because the procedural risks of myectomy are similar, and there is concern about the long term consequences of ablation and the proarrhythmic potential of the septal scar [12,13]. For some patients, surgery and alcohol ablation may not be considered viable alternatives because of advanced age or co-morbidities. In such patients, DDD pacing may offer a less invasive approach [8,10]. In addition, DDD pacing therapy permits more aggressive drug treatment by obviating the concern for drug-induced bradycardia [10].

This was an acute, proof-of-concept study, performed in the catheterization laboratory. It remains to be seen if combined DDD pacing and disopyramide offers more prolonged gradient reduction and symptom relief than either approach alone. Although the effects of temporary pacing at the time of catheterization are often not predictive of long-term outcome, previous studies showed that there is a correlation between the acute change in gradient by DDD pacing and the gradient at long-term follow-up [6]. The hemodynamic data in the present sturdy were obtained in the rest supine state and this study did not examine the effect of DDD pacing and disopyramide during exercise or with provocation.

In conclusion, we have demonstrated synergy between DDD pacing and disopyramide for LVOT gradient reduction in obstructive HCM. Study of the long-term effects of this combined therapy would be the next step to ascertain clinical utility.

Acknowledgment

We express our appreciation to Katsunori Shimada (STATZ Institute, Inc., Tokyo, Japan) for expert statistical assistance.

References

[1] Maron MS, Olivotto I, Betocchi S, et al. Effect of left ventricular outflow tract obstruction on clinical outcome in hypertrophic cardiomyopathy. N Engl J Med 2003;348:295–303.
[2] Pollick C. Disopyramide in hypertrophic cardiomyopathy. II. Noninvasive assessment after oral administration. Am J Cardiol 1988;62:1252–5.
[3] Pollick C, Kimball B, Henderson M, Wigle ED. Disopyramide in hypertrophic cardiomyopathy. I. Hemodynamic assessment after intravenous administration. Am J Cardiol 1988;62:1248–51.
[4] Sherrid M, Delia E, Dwyer E. Oral disopyramide therapy for obstructive hypertrophic cardiomyopathy. Am J Cardiol 1988;62:1085–8.
[5] Sherrid MV, Barac I, McKenna WJ, et al. Multicenter study of the efficacy and safety of disopyramide in obstructive hypertrophic cardiomyopathy. J Am Coll Cardiol 2005;45:1251–8.
[6] Fananapazir L, Epstein ND, Curiel RV, Panza JA, Tripodi D, McAreavey D. Long-term results of dual-chamber (DDD) pacing in obstructive hypertrophic cardiomyopathy. Evidence for progressive symptomatic and hemodynamic improvement and reduction of left ventricular hypertrophy. Circulation 1994;90:2731–42.
[7] Kappenberger L, Linde C, Daubert C, et al. Pacing in hypertrophic obstructive cardiomyopathy. A randomized crossover study. PIC study group. Eur Heart J 1997;18:1249–56.
[8] Maron BJ, Nishimura RA, McKenna WJ, Rakowski H, Josephson ME, Kieval RS. Assessment of permanent dual-chamber pacing as a treatment for drug-refractory symptomatic patients with obstructive hypertrophic cardiomyopathy. A randomized, double-blind, crossover study (M-PATHY). Circulation 1999;99:2927–33.
[9] Nishimura RA, Trusty JM, Hayes DL, et al. Dual-chamber pacing for hypertrophic cardiomyopathy: a randomized, double-blind, crossover trial. J Am Coll Cardiol 1997;29:435–41.
[10] Maron BJ, McKenna WJ, Danielson GK, et al. American College of Cardiology/European Society of Cardiology clinical expert consensus document on hypertrophic cardiomyopathy. A report of the American College of Cardiology Foundation Task Force on Clinical Expert Consensus Documents and the European Society of Cardiology Committee for Practice Guidelines. J Am Coll Cardiol 2003;42:1687–713.
[11] Nagueh SF, Ommen SR, Lakkis NM, et al. Comparison of ethanol septal reduction therapy with surgical myectomy for the treatment of hypertrophic obstructive cardiomyopathy. J Am Coll Cardiol 2001;38:1701–6.
[12] Maron BJ. Surgery for hypertrophic obstructive cardiomyopathy: alive and quite well. Circulation 2005;111:2016–8.
[13] Seggewiss H, Gleichmann U, Faber L, et al. Percutaneous transluminal septal myocardial ablation in hypertrophic obstructive cardiomyopathy: acute results and 3-month follow-up in 25 patients. J Am Coll Cardiol 1998;31:252–8.

Please cite this article as: Minami Y, et al, Synergistic effect of dual chamber pacing and disopyramide in obstructive hypertrophic cardiomyopathy, Int J Cardiol (2008), doi:10.1016/j.ijcard.2008.11.088

Experimental Studies

Noninvasive Detection of Cardiac Repair After Acute Myocardial Infarction in Rats by ^{111}In Fab Fragment of Monoclonal Antibody Specific for Tenascin-C

Kenichi ODAKA,[1] MD, Tomoya UEHARA,[2] PhD, Yasushi ARANO,[2] PhD, Sayaka ADACHI,[2] BS, Hiroyuki TADOKORO,[1] MD, Katsuya YOSHIDA,[1] MD, Hiroshi HASEGAWA,[1] MD, Kyoko IMANAKA-YOSHIDA,[3] MD, Toshimichi YOSHIDA,[3] MD, Michiaki HIROE,[4] MD, Toshiaki IRIE,[5] PhD, Shuji TANADA,[5] MD, *and* Issei KOMURO,[1] MD

SUMMARY

Left ventricular (LV) remodeling after acute myocardial infarction (MI) causes heart failure, and thus it is important to evaluate cardiac repair as the early stage of LV remodeling. Tenascin-C (TNC), an extracellular matrix glycoprotein, is transiently and abundantly expressed in the heart during the early stage of tissue remodeling after MI. However, it is not expressed in healthy adult heart. This study was undertaken to develop a new noninvasive diagnostic technique to detect cardiac repair after acute MI using ^{111}In Fab fragment of a monoclonal antibody specific for TNC.

^{111}In-anti-TNC-Fab was injected intravenously in 13 rats at 1 (D1, $n = 3$), 3 (D3, $n = 5$), and 5 (D5, $n = 5$) days after producing MI and in 5 sham-operated rats (S). We performed autoradiography and dual-isotope single-photon emission computed tomography imaging (SPECT) of ^{111}In-anti-TNC-Fab and ^{99m}Tc methoxyisobutyl isonitrile (MIBI).

The radioactivity in the heart was significantly higher in D (D1, 0.45 ± 0.06% injected-dose/g; D3, 0.64 ± 0.12; D5, 0.38 ± 0.07) than S (0.27 ± 0.06, $P < 0.01$ versus D1 and D3, $P < 0.05$ versus D5). By autoradiography, higher radioactivities were observed in the infarcted area than in the noninfarcted area of MI hearts. Dual-isotope SPECT demonstrated the regional myocardial uptake of ^{111}In-anti-TNC-Fab, which was complementary to the perfusion image.

The results of the present study indicated that we can localize the infarcted region in the heart by *ex vivo* and *in vivo* imaging methods using ^{111}In-anti-TNC-Fab, and suggested the potential usefulness of noninvasive detection of cardiac repair. (Int Heart J 2008;

From the [1] Department of Cardiovascular Science and Medicine, Chiba University Graduate School of Medicine, [2] Department of Molecular Imaging and Radiotherapy, Chiba University Graduate School of Pharmaceutical Sciences, Chiba, [3] Department of Pathology, Mie University School of Medicine, Mie, [4] Department of Nephrology and Cardiology, International Medical Center of Japan, Tokyo, and [5] Department of Medical Imaging, National Institute of Radiological Sciences, Chiba, Japan.

Address for correspondence: Issei Komuro, MD, Department of Cardiovascular Science and Medicine, Chiba University Graduate School of Medicine, 1-8-1-M4 Inohana, Chuo-ku, Chiba, Chiba 260-8670, Japan.

This study was supported by the Melvin Judkins Young Investigator Award of the American Heart Association, a research grant for PET and SPECT studies from the National Institute of Radiological Sciences of Japan, and Grants-in-Aid for Scientific Research and for Young Scientists from the Ministry of Education, Science, Sports, and Culture of Japan.

Received for publication April 9, 2008.

Revised and accepted June 19, 2008.

49: 481-492)

Key words: Myocardial infarction, Cardiac repair, Fab fragment, Tenascin-C, Extracellular matrix, Single-photon emission computed tomography

MYOCARDIAL infarction (MI) is a very common and serious disease. The infarct size is a major predictor of left ventricular (LV) remodeling following MI. Since LV remodeling causes progression to heart failure and is a major predictor of morbidity and mortality, prevention of the progression of LV remodeling following MI is an important therapeutic approach for heart failure.[1] Thus, the quantitative examination and early treatment of LV remodeling are important issues for cardiologists. In spite of the development of various diagnostic modalities, early and precise diagnosis of LV remodeling after MI remains impossible.

Significant morphological alterations involving both myocyte loss and interstitial space myocardial tissue remodeling have been described in the infarcted area.[2,3] These structural changes are considered to be important factors responsible for the progression of the expansion of infarcted LV. Tenascin-C (TNC), an extracellular matrix glycoprotein which reorganizes the cell shape or arrangement, is transiently and abundantly expressed in the heart during cardiac repair as the early stage of tissue remodeling after acute MI within the border zone area.[4] However, it is not expressed in healthy adult heart. These observations suggest that TNC is actively involved in LV remodeling after MI and could be used as a molecular marker to detect cardiac repair.[5,6]

In the present study, we injected the ^{111}In Fab fragment of a monoclonal antibody specific for TNC into acute MI rats and sham-operated rats, and measured its biodistribution. The localization of the radioactivity in the myocardium was also analyzed by *in vivo* imaging (single-photon emission computed tomography [SPECT]) and *ex vivo* imaging (autoradiography).

METHODS

Acute myocardial infarction model: Forty-four 7-week-old male Wistar rats purchased from Japan SLC, Inc. (Shizuoka, Japan) were used in our protocol, which was approved by the Special Committee on Animal Welfare of the National Institute of Radiological Sciences. The animals were anesthetized with halothane (2%/L) and then underwent a tracheotomy. The rats were ventilated by positive pressure through endotracheal tubes attached to a Harvard small animal respirator (SN-480-5; Shinano, Tokyo). Left thoracotomy was performed and the left descending coronary artery was ligated. In sham-operated rats, a left thoracotomy

was performed and the coronary artery was incompletely ligated. Two normal rats were also included to compare to other models. No antibiotic medication was used to prevent allergic inflammation.

Antibody: A mouse monoclonal antibody against TNC, clone 4F10TT, was raised by immunization of a TNC-null mouse[7-9] with purified human TNC[10] as described previously.[11] Isolated splenic cells from a TNC-null mouse immunized with TNC were fused with SP2/0 myeloma cells. Immunoglobulin was purified from the culture supernatant of hybridoma cell clone 4F10TT cultured in serum-free media. The Fab fragment was prepared using a Fab preparation kit (ImmunoPure® IgG1 Fab and F(ab')$_2$ Preparation Kit, Pierce, Rockford, Il).

As a nonspecific control antibody, an isotype-matched monoclonal antibody against the V protein of parainfluenza virus type II (clone 53-1, isotype IgG1; kindly provided by the Department of Microbiology, Mie University School of Medicine) was also digested to the Fab fragment as described above.

Radiolabeling with ^{111}In: The bifunctional chelating agent 1-(4-isothiocyanatobenzyl)diethylenetriamine penta acetic acid (SCN-Bz-DTPA) was synthesized according to the method of Cummins, *et al.*[12] Fab-SCN-Bz-DTPA was prepared according to the procedure as reported previously, with slight modifications.[13] To a solution of Fab (5 mg/mL) in borate buffer (0.05 M, pH 8.5 100 μL), a 15 molar excess of SCN-Bz-DTPA in borate buffer (0.05 M, pH 8.5, 10 μL) was added. After incubating for 15 hours at 37°C, the conjugate was purified by centrifugation using a Sephadex G-50 column (Pharmacia Biotech KK, Tokyo) equilibrated with 0.1 M acetate buffer (pH 6.0). The purified conjugates were labeled with ^{111}In, as previously reported.[14] ^{111}In Fab fragments were purified using Sephadex G-50 equilibrated with 0.1 M phosphate buffer (pH 6.0). The radiochemical purity of ^{111}In Fab fragments was determined by cellulose acetate electrophoresis. Under similar conditions, unpurified conjugates were labeled with ^{111}In and analyzed by cellulose acetate electrophoresis to estimate the number of SCN-Bz-DTPA groups attached per Fab fragment.[15]

Nonlabeled anti-TNC-Fab solution was added to obtain the desired level of ^{111}In-anti-TNC-Fab radioactivity. Therefore, 50 μg of anti-TNC-Fab was injected into every rat.

Biodistribution study: Thirteen MI rats and 5 sham-operated rats were injected intravenously through the tail vein with 50 μg (111 KBq) of ^{111}In-anti-TNC-Fab in 300 μL of saline solution. The animals were euthanized 6 hours after the tracer injection. Hearts, other organs (lung, liver, kidney, spleen, chest with sutured incision after thoracotomy, and hindlimb muscle), and blood were weighed and then the radioactivity was counted with the blood samples. To determine the uptake in the infarcted area, the whole heart was divided into infarcted and noninfarcted areas. The infarcted area included the white colored muscle and normal colored

margin. The percentage of the injected dose of the radioactivity per gram tissue weight (%ID/g) was calculated as follows:

%ID/g = cpm of tissue / cpm of ^{111}In-anti-TNC Fab / tissue weight × 100 × body weight / 250

The specific uptake of anti-TNC-Fab in acute MI rats was also estimated by comparing the radioactivity distribution of the same amounts (111 KBq, 50 μg) of ^{111}In-anti-TNC-Fab ($n = 5$) or ^{111}In-nonspecific Fab ($n = 6$) 3 days after producing MI. All data are presented as the mean ± SD. The sham-operated and MI groups were compared using the unpaired Student t test.

Histopathologic and quantitative autoradiographic study: Rats were administered similar amounts (740 KBq, 50 μg) of ^{111}In-anti-TNC-Fab. At 6 hours after injection, the hearts were excised and embedded in Tissue-Tek optimum cutting temperature compound. Five μm thick sections were stained with hematoxylin-eosin stain or van Gieson stain. Adjacent heart sections of 20 μm thickness were exposed to the imaging plate of an image analyzer (BAS-1800 system, Fuji Film Co Ltd, Tokyo) for autoradiography.

Immunohistochemical staining: Immunohistochemical staining of tissue sections was performed as described previously.[4] In brief, the sections were first incubated with the primary antibody 4F10TT (1 μg/mL) and then with peroxidase-conjugated anti-mouse IgG (1:500, MBL Aichi, Japan). After the sections were washed, a diaminobenzidine/H_2O_2 solution was used to demonstrate antibody binding.

In vivo SPECT imaging: ^{111}In-anti-TNC-Fab *in vivo* imaging was performed in rats using dual-isotope SPECT as described previously.[16] The SPECT system consisted of a 3-headed γ-camera (Toshiba GCA 9300A) equipped with 1.0-mm pinhole collimators. ^{111}In-anti-TNC-Fab (3.7 MBq, 50 μg) was injected intravenously, followed by the injection of 37 MBq of ^{99m}Tc methoxyisobutyl isonitrile (MIBI) (DRL, Tokyo) 5.5 hours later. Thirty minutes later, the rats were anesthetized by an intraperitoneal injection of pentobarbital (30 μg/g), and 60-minute data acquisition was performed at 120 seconds per view with stepwise rotation for each 4 degrees over 120 degrees and with multiple peak acquisition (15% windows for the ^{99m}Tc and both ^{111}In peaks). The matrix was 128 × 128 for data acquisition and for the image display with 0.6-mm pixel size. Image data analysis was performed with transverse dual-isotope SPECT imaging. Visual interpretation of SPECT images was performed by 2 experienced observers. Myocardial uptake of ^{111}In-anti-TNC-Fab was defined as cardiac repair. Myocardial perfusion defect of ^{99m}Tc-MIBI was defined as MI. The rats were divided into 4 groups according to cardiac repair and MI. Fisher's exact test was used to determine the concordance between cardiac repair and MI. A $P < 0.05$ was considered significant.

RESULTS

Acute myocardial infarction model: No symptom of infection was seen in the rats throughout the present study. Five rats died within 30 minutes of ligation. Two rats died between 30 minutes and one day after ligation.

In vivo biodistribution of ^{111}In-anti-TNC-Fab: The SCN-Bz-DTPA group was attached to the Fab fragment for TNC at the ratio of 0.8-1.3. After purification by centrifugation, Fab-SCN-Bz-DTPA-^{111}In was obtained with radiochemical purity of over 90%. Biodistribution was examined in the rats at 1 ($n = 3$), 3 ($n = 5$), and 5 ($n = 5$) days after producing MI and sham-operation ($n = 5$). The tissue uptake of ^{111}In-anti-TNC-Fab is presented as a percentage of the injected dose per gram tissue (Table I). Rapid clearance of the radioactivity from the circulation was observed with ^{111}In-anti-TNC-Fab in both acute MI and sham-operated rats (< 1% at 6 hours after injection). The uptake was the highest in the kidney, followed by the spleen and liver. The average radioactivity of the whole heart was significantly higher in acute MI rats than in sham-operated rats. The accumulation of injected anti-TNC-Fab increased gradually and peaked at the third day in the in-

Table I. Biodistribution of ^{111}In-Anti-Tenascin-C-Fab and ^{111}In-Nonspecific Fab

Tissue	TNC Ab MI (1 day) $n = 3$	TNC Ab MI (3 days) $n = 5$	TNC Ab MI (5 days) $n = 5$	TNC Ab Sham-operated (5 days) $n = 5$	Nonspecific Ab MI (3 days) $n = 6$
Blood	0.33 ± 0.02	0.35 ± 0.03	0.38 ± 0.03	0.37 ± 0.04	0.37 ± 0.05
Heart	0.45 ± 0.06*	0.64 ± 0.12*	0.38 ± 0.07†§	0.27 ± 0.06	0.30 ± 0.08
Lung	0.29 ± 0.02	0.56 ± 0.17	0.46 ± 0.04‡	0.39 ± 0.09	0.34 ± 0.10
Liver	2.87 ± 0.36§	3.22 ± 0.30	3.04 ± 0.54	3.37 ± 0.70	0.49 ± 0.04
Kidney	12.94 ± 2.26	15.47 ± 1.76	14.22 ± 1.44	14.10 ± 2.12	15.00 ± 2.29
Spleen	3.12 ± 0.57	2.91 ± 0.67	3.02 ± 0.21	3.16 ± 0.93	0.62 ± 0.27
Muscle	0.02 ± 0.00	0.03 ± 0.00§	0.03 ± 0.00	0.02 ± 0.00	0.07 ± 0.05
Chest injury	0.53 ± 0.08§	0.96 ± 0.22*	1.23 ± 0.31*‡	0.54 ± 0.14	0.53 ± 0.32
Infarcted area (heart)	0.78 ± 0.08*¶	1.14 ± 0.13*	0.62 ± 0.15*¶	0.28 ± 0.03	0.36 ± 0.08
Noninfarcted area (heart)	0.26 ± 0.06	0.38 ± 0.10	0.24 ± 0.03§	0.27 ± 0.08	0.27 ± 0.11
Infarcted / Noninfarcted	3.2 ± 0.9*	3.1 ± 0.6*	2.5 ± 0.4*	1.1 ± 0.3	1.4 ± 0.4
Infarcted area /Blood	2.4 ± 0.4*¶	3.3 ± 0.2*	1.6 ± 0.4*¶	0.8 ± 0.2	1.0 ± 0.2

MI indicates myocardial infarction and Muscle, hindlimb skeletal muscle.

Values at each time point represent mean ± SD of percentage of injected dose per gram tissue weight.

*$P < 0.01$ versus sham-operated rats, †$P < 0.01$ versus rats 3 days after producing myocardial infarction, ‡$P < 0.01$ versus rats one day after producing myocardial infarction.

§$P < 0.05$ versus sham-operated rats, ¶$P < 0.05$ versus rats 3 days after producing myocardial infarction, ¶$P < 0.05$ versus rats one day after producing myocardial infarction.

farcted heart. The uptake of ^{111}In-anti-TNC-Fab was significantly higher in the infarcted area than in the noninfarcted area in acute MI rats (Table I), suggesting that the uptake was specific for the infarcted area.

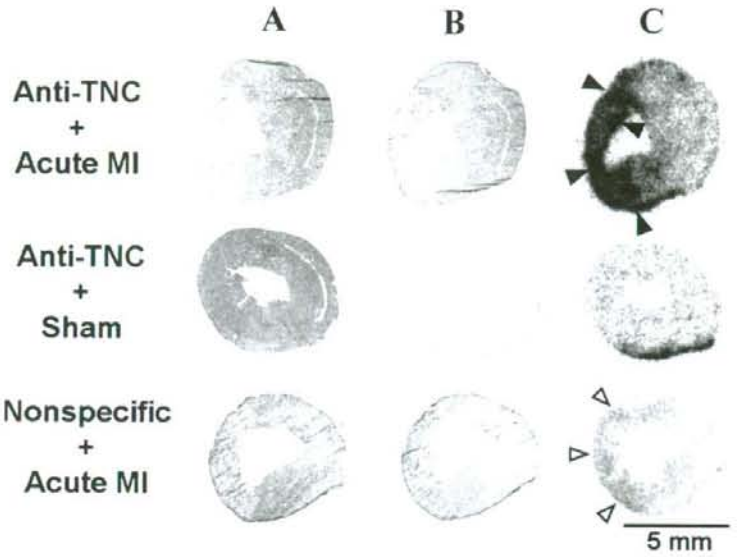

Figure 1. Histology and autoradiography. Hematoxylin-eosin staining (**A**), van Gieson staining (**B**), and autoradiography (**C**) of adjacent sections from hearts of acute MI rats (upper panels and lower panels) and sham-operated rats (middle panels). Upper panels and middle panels show the heart sections from rats administered ^{111}In-anti-TNC-Fab. Lower panels show heart sections from rats that received intravenous injection of ^{111}In-nonspecific Fab. Accumulation of ^{111}In-anti-TNC-Fab was observed in the border zone of acute MI heart (black arrowheads). In the heart of sham-operated rats, the uptake was observed in the epicardial region which was adjacent to the operated chest. Equivocal accumulation of ^{111}In-nonspecific Fab was observed in the infarcted region of MI heart (white arrowheads).

Figure 2. Immunohistochemical staining. Immunohistochemical staining with anti-TNC-Fab shows extensive expression of TNC in the border zone of acute MI heart (**A**, brown). Sham-operated rat heart showed no myocardial expression of TNC, but slight expression was seen in the epicardium which indicated inflammation (**B**, arrowheads) caused by left thoracotomy for the sham-operation. Normal rat heart showed no myocardial expression of TNC (**C**).